

UNCLASSIFIED

C.2



RESEARCH MEMORANDUM

AERODYNAMIC HEAT TRANSFER AND ZERO-LIFT DRAG OF A FLAT
WINDSHIELD CANOPY ON THE NACA RM-10 RESEARCH VEHICLE

AT HIGH REYNOLDS NUMBERS FOR A FLIGHT MACH

NUMBER RANGE FROM 1.5 TO 3.0

By Sherwood Hoffman and Leo T. Chauvin

Langley Aeronautical Laboratory
Langley Field, Va.

LIBRARY COPY

SEP 28 1956

LANGLEY AERONAUTICAL LABORATORY
LIBRARY NACA
LANGLEY FIELD, VIRGINIA

CLASSIFIED DOCUMENT

This material contains information affecting the National Defense of the United States within the meaning of the espionage laws, Title 18, U.S.C., Secs. 793 and 794, the transmission or revelation of which in any manner to an unauthorized person is prohibited by law.

NATIONAL ADVISORY COMMITTEE FOR AERONAUTICS

WASHINGTON

September 26, 1956

CLASSIFICATION CHANGED

UNCLASSIFIED

To

By authority

~~CONFIDENTIAL~~



NATIONAL ADVISORY COMMITTEE FOR AERONAUTICS

RESEARCH MEMORANDUM

AERODYNAMIC HEAT TRANSFER AND ZERO-LIFT DRAG OF A FLAT
WINDSHIELD CANOPY ON THE NACA RM-10 RESEARCH VEHICLE
AT HIGH REYNOLDS NUMBERS FOR A FLIGHT MACH

NUMBER RANGE FROM 1.5 TO 3.0

By Sherwood Hoffman and Leo T. Chauvin


SUMMARY

The aerodynamic heat-transfer properties and zero-lift drag of a typical pilot's canopy have been determined by a rocket-model flight test through a Mach number range from about 1.5 to 3.0 and corresponding Reynolds number range from approximately 18×10^6 to 59×10^6 , based on the length between the fuselage nose and canopy. The canopy had a 63° sweptback flat windshield, circular cross section, and an equivalent body fineness ratio of 7.0. Two canopies were symmetrically mounted above and below the NACA RM-10 research vehicle at the 32.8-percent fuselage station for the test.

The dimensionless heat-transfer coefficients or Stanton numbers increased in value along the face of the canopy, for Mach numbers at and above 2, and then decreased rapidly in the region of high expansion just behind the windshield. The Stanton numbers for the canopy afterbody decreased with increasing Mach number and Reynolds number whereas such effects were not evident for the forward half of the canopy. The theoretical flat-plate Stanton numbers based on local conditions were of the same order of magnitude as the experimental values at the forward and midcanopy stations. The canopy plus interference drag coefficient was about 0.1 between Mach numbers 1.4 and 1.8 and then increased with Mach number to a value of 0.28 at Mach number 3.0.

INTRODUCTION

As part of a general research program of the National Advisory Committee for Aeronautics to determine the heat-transfer properties of aircraft components, the Langley Pilotless Aircraft Research Division has tested a typical pilot's canopy on the NACA RM-10 research vehicle



at its test station at Wallops Island, Va. The present paper presents experimental heat-transfer coefficients and zero-lift drag for the canopy up to Mach number 3.0 and Reynolds number up to 59×10^6 based on the length between the fuselage nose and canopy. In order to aid the designer in estimating the heat-transfer coefficient, the experimental data are compared with that predicted by flat-plate theory based on local conditions. The aerodynamic heating and drag data presented were obtained from telemetered measurements of wall-temperature distribution, pressure distribution, and acceleration in flight. Some recent flight test investigations of the aerodynamic heat transfer for other aircraft components are given in references 1 to 7.

SYMBOLS

A_C	maximum cross-sectional area of one canopy, ft^2
A_F	maximum cross-sectional area of fuselage, ft^2
a	tangential acceleration, ft/sec^2
C_D	total drag coefficient based on A_F
ΔC_D	$= C_{D_{\text{fuselage+canopies}}} - C_{D_{\text{fuselage}}}$
C_p	pressure coefficient, $\frac{p_v - p_l}{q_l}$
c_p	specific heat of air at constant pressure, $\text{Btu}/\text{slug}, ^\circ\text{F}$
c_w	specific heat of wall material, $\text{Btu}/\text{lb}, ^\circ\text{F}$
g	acceleration due to gravity, $32.2 \text{ ft}/\text{sec}^2$
h	aerodynamic heat-transfer coefficient, $\text{Btu}/\text{sec-ft}^2, ^\circ\text{F}$
L	length of fuselage, in.
l	length of canopy, in.
M	Mach number
N_{Pr}	Prandtl number

N_{St}	Stanton number, $h/(c_p \rho V)_v$
δN_{St}	probable error in Stanton number
p	static pressure, lb/ft ²
q	dynamic pressure, lb/ft ²
R	Reynolds number
R.F.	recovery factor, $\frac{T_{aw} - T_v}{T_{so} - T_v}$
r	radius of fuselage, in.
r_c	radius of canopy, in.
T	temperature, °R
t	time from start of flight, sec
V	velocity, ft/sec
W	weight of model during deceleration, lb
X	station measured from fuselage nose, in.
x	station measured from canopy leading edge, in.
y_r	ordinate to canopy reference line, in.
γ	ratio of specific heats
ρ	density of air, slugs/ft ³
ρ_w	specific weight of wall, lb/ft ³
τ	wall thickness, ft
θ	angle between flight path and horizontal, deg
ϕ	canopy polar angle measured from top of canopy, deg

Subscripts:

aw	adiabatic wall
w	wall (skin)
l	free-stream conditions
so	free-stream stagnation
v	just outside boundary layer

MODEL AND INSTRUMENTATION

Details, dimensions, and photographs of the configurations tested are given in figures 1 and 2. The NACA RM-10 research vehicle was used as the fuselage of the configuration. This body was derived from a parabolic arc of revolution of fineness ratio 15 by cutting off part of the pointed stern to allow space for the rocket jet. The resulting fuselage had a fineness ratio of 12.2, maximum body diameter of 12 inches, and was equipped with a 6.25-inch Deacon rocket motor. The configuration was stabilized by four 60° sweptback, untapered fins of total aspect ratio 2.04. The airfoil of the fins consisted of a 10-percent-thick circular-arc cross section normal to the leading edge or 5 percent thick in the streamwise direction. The skin of the fuselage was made of spun magnesium alloy to which the cast magnesium fins were attached. All the surfaces were smooth and highly polished.

The canopy was designed to have a flat windshield sweptback 63° , circular cross section, and an equivalent body fineness ratio of 7.0. Two canopies were symmetrically located above and below the fuselage for the test. The windshields intersected the fuselage surface at the 48-inch station of the body. Each canopy was constructed of nickle (electroformed), had a polished surface, and was insulated from the fuselage by a phenoline slab. Table I lists the wall (skin) thickness at the canopy stations that were selected for the wall-temperature measurements.

The model was equipped with 11 channels of telemetering to transmit the measured wall temperatures, pressures, and drag acceleration to a ground receiving station. The temperature pickup was commutated every 0.2 second to transmit temperature measurements at 12 canopy stations. The stations selected are shown in figure 1(b) and are identified in terms of nondimensional canopy station x/l and polar angle ϕ measured from the top of the canopy (meridian plane). The skin temperatures were measured by means of iron constantan thermocouples (no. 30 gage) welded to the inner surface of one of the canopies. The accuracy of the

temperatures recorded was within $\pm 10^\circ$ F. A more complete discussion of the general methods of the temperature telemetering techniques employed is presented in reference 1.

Nine of the channels transmitted continuous readings of pressure on the other canopy at stations corresponding to temperature stations as is shown in figure 1(b). The pressure orifices were made of 0.125-inch outside diameter (0.055-inch inside diameter) copper tubing. The instrumentation used had a time-lag constant of about 0.007 second, which was sufficiently small to allow pickup of the rapid changes in pressure obtained during accelerating flight. The pressure cells were connected to read differential pressures based on an estimated pressure gradient over the canopy. Since the accuracy of the pressure instrumentation was about ± 2 percent of the full-scale deflection of each cell, this arrangement greatly reduced the error by making it possible to use small-scale ranges for most of the stations. The only absolute-pressure reading taken was on the windshield at $x/l = 0.072$ and $\phi = 0^\circ$, whereas the remaining pressure readings were relative to the orifice giving the next highest estimated reading.

METHOD AND PROCEDURES

Test

The model was tested at the Langley Pilotless Aircraft Research Station at Wallops Island, Va. through a continuous range of Mach number from about 1.5 to 3.0 and Reynolds number from approximately 55×10^6 to 180×10^6 based on total fuselage length as is shown in figure 3(a). The maximum Mach number was attained through propulsion by a two-stage rocket system (fig. 2(c)). The first stage, which consisted of two 6.25-inch Deacon rocket motors burning simultaneously, boosted the model to Mach number 1.6. After burn-out of this stage, the booster drag separated from the model. The model coasted for about 7 seconds after which the second stage, which was incorporated in the fuselage, accelerated the configuration to Mach number 3.13. Velocity and trajectory data were obtained from the CW Doppler velocimeter and the NACA modified SCR-584 tracking radar unit, respectively. A survey of atmospheric conditions including winds aloft was made by rawinsonde measurements from an ascending balloon that was released before each test. The free-stream conditions for the test are presented in figure 3(b).

Data Reduction

From the measurements of wall temperature and pressure, time histories, and flight conditions, the data were reduced to Stanton number

from the following relation:

$$N_{St} (c_p \rho V)_v = \frac{\tau \rho_w c_w}{T_{aw} - T_w} \left(\frac{dT_w}{dt} \right)$$

The above equation is valid for these tests because conduction and radiative heat losses were found to be negligible when compared to the total heat transferred to the canopy, with the possible exception of the measurements at stations (x/l) 0.214 and 0.241.

The thickness, density, and specific heat (ref. 8) of the material were known. The value of the specific heat for the nickel canopy varied nearly linearly from 0.112 Btu per pound per degree Fahrenheit at 200° F to 0.142 at 1500° F.

The adiabatic wall temperature was obtained from the expression

$$T_{aw} = R.F. (T_{so} - T_v) + T_v$$

where the recovery factor is assumed equal to $(N_{Pr})^{1/3}$ based on T_w for all turbulent flow over the canopy. The assumption of turbulent flow was based on the high values of local Reynolds number ahead of the canopy and also from tests of the body alone in reference 2. The values of recovery factor used, based on $(N_{Pr})^{1/3}$, varied between 0.87 and 0.89 throughout the test range. No experimental recovery factors were obtained because of the accuracy of the measurements.

In order to determine the local flow conditions outside of the boundary layer at the canopy stations, such as $(c_p \rho V)_v$ and T_v , the shock-wave losses and local conditions just forward of the canopy windshield had to be estimated. The total shock-wave losses were obtained at several representative flight Mach numbers by assuming a conical shock at the fuselage nose and an attached two-dimensional oblique shock at the canopy windshield above a free-stream Mach number of 2.2. Below this Mach number, a normal shock was assumed for the windshield instead of a detached oblique shock. The local flow conditions on which the windshield shock waves are based were determined from pressure measurements about the fuselage alone in reference 9 for comparable Mach number and Reynolds number ranges.

The values of total drag coefficient, based on the fuselage frontal area, were obtained during decelerating flight with the expression:

$$C_D = - \frac{W}{q_1 g A_F} (a + g \sin \theta)$$

For comparative purposes, the drag was evaluated with the decelerations as determined by the drag accelerometer and by differentiating the velocity time curve of the CW Doppler radar. A more complete discussion on the method of reducing the drag data is given in reference 10.

ACCURACY

The probable error in determining the heat-transfer coefficient and Stanton number utilizing the present experimental technique is discussed in detail in reference 3. In general, the error is dependent on the accuracy of the measurements obtained during the flight test, the accuracy of determining the local flow conditions outside the boundary layer, and the error due to neglecting the contributions of radiation and conduction along the skin. Reference 3 shows that the probable error in Stanton number may be approximated from the following expression:

$$\frac{\delta N_{St}}{N_{St}} \approx \left[\frac{403}{(T_{aw} - T_w)^2} + \frac{1}{\left(\frac{dT_w}{dt}\right)^2} + 0.0022 \right]^{1/2}$$

It is evident from the above equation that the Stanton number becomes too inaccurate when $T_{aw} - T_w$ and dT_w/dt approach 0. An example of the accuracy is presented in figure 4 for a typical measuring station ($x/l = 0.894$, $\phi = 0^\circ$). Figure 4(a) shows the probable error as a function of $T_{aw} - T_w$. The variations of $T_{aw} - T_w$ through the second boost and coast stage of the test are given in figure 4(b). Figure 4(c) shows the computed Stanton numbers for this station and an accuracy band based on the aforementioned equation. The largest and inadmissible errors were obtained during coasting flight for both the first and second coast periods. In comparison, the accuracy during the second acceleration boost (10 sec to 13.1 sec) was particularly good and, in general, varied within a maximum error of ± 10 percent of the measured values. As a consequence, the analysis presented herein is primarily based on the data obtained

during the latter acceleration period, and comparisons are made with deceleration data for the second coast period whenever the accuracy of the measurements from this last period appears good.

The error in pressure coefficient and total drag coefficient, based on instrument accuracy, was estimated to be ± 0.015 and ± 0.01 , respectively. The free-stream Mach number also was estimated to be within ± 0.01 through most of the Mach number range.

RESULTS AND DISCUSSION

Canopy Temperature Distribution

The variations of measured wall temperature with time for the second boost and coast stage of the flight test are presented in figure 5. This time interval covers the complete Mach number range for both acceleration and deceleration data. The low supersonic data obtained from the first part of the test (below 10 sec) gave large errors in the determination of Stanton number, based on the accuracy analysis of reference 3, and have been omitted. The temperature distribution over the canopy during the acceleration period (10 to 13.1 sec) where the skin is being heated is presented in figure 6 for free-stream Mach numbers of 1.5, 2.0, 2.2, 2.5, and 3.0. The curves faired through the test points at $\phi = 0^\circ$ illustrate the variation of skin temperature over the top of the canopy. As would be expected, the highest temperatures are obtained on the flat windshield where the compression is greatest at each Mach number. The fairings used in figure 6(b) are arbitrary and only intended as an aid in showing the general variation of skin temperature along the side of the canopy. These temperature distributions are typical also of those obtained for the decelerating part of the flight where, in general, the skin is being cooled.

Canopy Pressure Distribution

The measured pressures on the canopy are presented in coefficient form for the flight-test time interval from approximately 10 to 25 seconds in figure 7. The solid curves shown represent the pressure coefficients for which accurate measurements were obtained. The dashed portions of the curves identify those parts of the flight-test range where the pressure coefficients have been estimated from either off-scale measurements or extrapolations.

The pressure distribution along the top of the canopy and at the few points on the side of the canopy for the acceleration period (10 to 13.1 sec) is shown in figure 8. The pressure coefficients obtained from

the second coast period (not shown) agree well with the acceleration data between Mach numbers from about 2.2 to 3.0. The agreement at the lower Mach numbers was within 20 percent. The deceleration data appear to be less accurate because of the off-scale readings and their possible effect on the calibration of the pressure cells. The values of peak-pressure coefficient at the forward station ($x/l = 0.072$, $\phi = 0^\circ$) on the windshield may be shown to be approximately the same as that for a wedge with an oblique shock wave, based on local flow conditions, when the shock is attached. For free-stream Mach numbers below 2.2, where the windshield shock is detached, the values of C_p for an assumed wedge would be considerably higher than for the inclined flat windshield. The drop in pressure along the windshield was obtained also in a previous investigation (ref. 11) and appears to result from both the expansions around the edges of the windshield and interference from the fuselage. This test and reference 11 indicate that only small increases in windshield pressure coefficient are obtained from increasing Mach number at zero lift.

The values of the parameter $(c_p \rho V)_v$ as determined from the local conditions over the canopy for the same acceleration time interval mentioned above are presented in figure 9. Since pressure measurements were not taken at stations $x/l = 0.143$, $\phi = 0^\circ$; $x/l = 0.643$, $\phi = 0^\circ$; and $x/l = 0.241$, $\phi = 34.3^\circ$, the values shown for these stations were based on the estimated local pressure coefficient. The magnitude and distribution of $(c_p \rho V)_v$ for the decelerating data (not shown) are similar to those shown in the figure but are somewhat smaller in magnitude.

Heat-Transfer Coefficient

The distributions of heat-transfer coefficient for the canopy as determined for several Mach numbers during the time interval from 10 to 13.1 seconds are presented in figure 10. The heat-transfer coefficient along $\phi = 0^\circ$ drops markedly just behind the windshield and then becomes constant at a value of about 0.020 on the canopy afterbody regardless of Mach number. Although there are too few points to determine the variation of h along the side of the canopy (fig. 10(b)), the heat-transfer distributions along the side are somewhat similar to those at the top. At station 0.429, for instance, h is about equal to 0.02 at $\phi = 76.2^\circ$ as well as at 0° for Mach numbers of 2.0 and higher. The agreement obtained at these radial stations may be due to the fact that both points lie in the region of high expansion just behind the windshield. The apparent deviation in h for the side stations at $M = 1.5$ may have resulted from detachment of the shock from the windshield and/or inaccurate measurements at low supersonic speeds.

The nondimensionalized heat-transfer coefficients or Stanton numbers and the local Reynolds numbers for the top of the canopy are given in figures 11(a) and 11(b), respectively. The local Reynolds numbers are based on the length between the nose of the fuselage and each (pressure orifice) station and the local conditions outside the boundary layer. The comparison shows that the Stanton number increases along the face of the canopy at each Mach number at and above 2 and remains nearly constant at the lower Mach number. The Stanton numbers decrease rapidly in the region of high expansion just behind the canopy windshield. The results also show that the level of Stanton number on the rear half of the canopy decreases significantly with increasing Mach number and Reynolds number, whereas such effects were not obtained for the forward half of the canopy. The Stanton numbers and Reynolds numbers for the side of the canopy are given in figure 12. No conclusions are being made from the measurements at the few stations used. With the possible exception of the results at $M_1 = 1.5$ for the side stations, values of Stanton number given in figures 11 and 12 are believed to be accurate within ± 10 percent.

The Stanton numbers and local Reynolds numbers along the top of the canopy for the acceleration period are compared with those obtained during decelerating flight (13.1 to 25 sec) and turbulent flat-plate theory (ref. 12) in figure 13. Since the skin temperatures are not isothermal, the theoretical values are intended to serve only as a datum or reference for engineering purposes. According to reference 13, the flat-plate Stanton numbers were taken as equal to 0.6 of the turbulent skin-friction coefficient based on local Reynolds number, Mach number, and heating conditions. At a free-stream Mach number 3.0 (fig. 13(a)), where the canopy is being heated for both the acceleration and deceleration results, the agreement for the two parts of the flight test is excellent along the canopy afterbody and fair near the forward part of the windshield. The Stanton number increases from about 9.3×10^{-4} to 12.8×10^{-4} along the canopy face during acceleration and from about 9×10^{-4} to 10×10^{-4} during the deceleration period. The theoretical flat-plate values are of the same order of magnitude as Ng_t for the forward part of the windshield and midsection of the canopy. The disagreement between the theory and test results is greatest at the rearmost stations of the windshield and afterbody of the canopy. At Mach number 2.5 (fig. 13(c)) the flight test results are compared for those stations where reasonable measurements were obtained for the deceleration data. The deceleration data are less accurate due to larger errors in the pressure coefficient and lower values of $T_{aw} - T_w$ than for the acceleration data. The flat-plate theory also indicates only a small effect of local Reynolds number (fig. 13(d)) and heating conditions T_w/T_v on the Stanton numbers obtained. At $M = 1.5$ in figure 13(e), where only the acceleration Ng_t is compared with the theory, the agreement is similar to that obtained for the higher Mach numbers.

Drag

The variations of total drag coefficient and canopy plus interference drag coefficient with Mach number are presented in figures 14(a) and 14(b), respectively. The accelerometer drag points shown were obtained from a signal received from the accelerometer at two receiving stations. The scatter of these points about the average drag curve indicates the accuracy of measurement. The drag curve for the body alone is an average curve as obtained from flight tests of several RM-10 bodies (ref. 9) through Reynolds number ranges that were similar to that of the present test. The canopy plus interference drag coefficient, based on total-canopy frontal area, was obtained from the difference in the average total drag curves given in figure 14(a). The variation of canopy drag with Mach number shows a nearly constant value of incremental drag of about 0.1 between Mach numbers 1.4 and 1.8. Thereafter, the canopy drag increases with Mach number to a value of 0.28 at Mach number 3.0. The drag for the canopy near Mach number 1.4 is low compared to the drags of similar canopies tested on pointed bodies in reference 14. This may be explained (ref. 14) by the fact that the canopy has both a low ratio of canopy to fuselage frontal area and a favorable location forward of the fuselage maximum diameter.

CONCLUSIONS

Supersonic convective heat transfer and zero-lift drag have been measured in free flight for a canopy having a 63° sweptback flat windshield on the NACA RM-10 research vehicle. The flight tests covered a range of Mach number varying from approximately 1.5 to 3.0 with Reynolds numbers varying from about 18×10^6 to 59×10^6 based on the length between the canopy windshield and fuselage nose. The results indicate the following conclusions:

1. For Mach numbers between 2 and 3, the Stanton numbers increased along the windshield of the canopy reaching maximum value at the end of the windshield. At lower Mach numbers, the Stanton numbers remained nearly constant along the face of the canopy.
2. The Stanton numbers just behind the windshield in the region of high expansion decreased rapidly at each test Mach number.
3. The level of Stanton number distribution on the rear half of the canopy decreased with increasing Mach number and Reynolds number, whereas no systematic effects due to Mach number and Reynolds number were obtained on the windshield.

4. Theoretical flat-plate heat-transfer coefficients based on local conditions were of the same order of magnitude as the experimental values at the forward windshield and midcanopy stations. The greatest disagreement was obtained at the rearmost windshield and canopy after-body stations.

5. Only small increases in windshield pressure coefficient were obtained by increasing the Mach number from 1.5 to 3.0.

6. The canopy plus interference drag coefficient was nearly constant at 0.1 between Mach numbers 1.4 and 1.8, thereafter increasing with Mach number to a value of 0.28 at Mach number 3.0.

Langley Aeronautical Laboratory,
National Advisory Committee for Aeronautics,
Langley Field, Va., June 19, 1956.

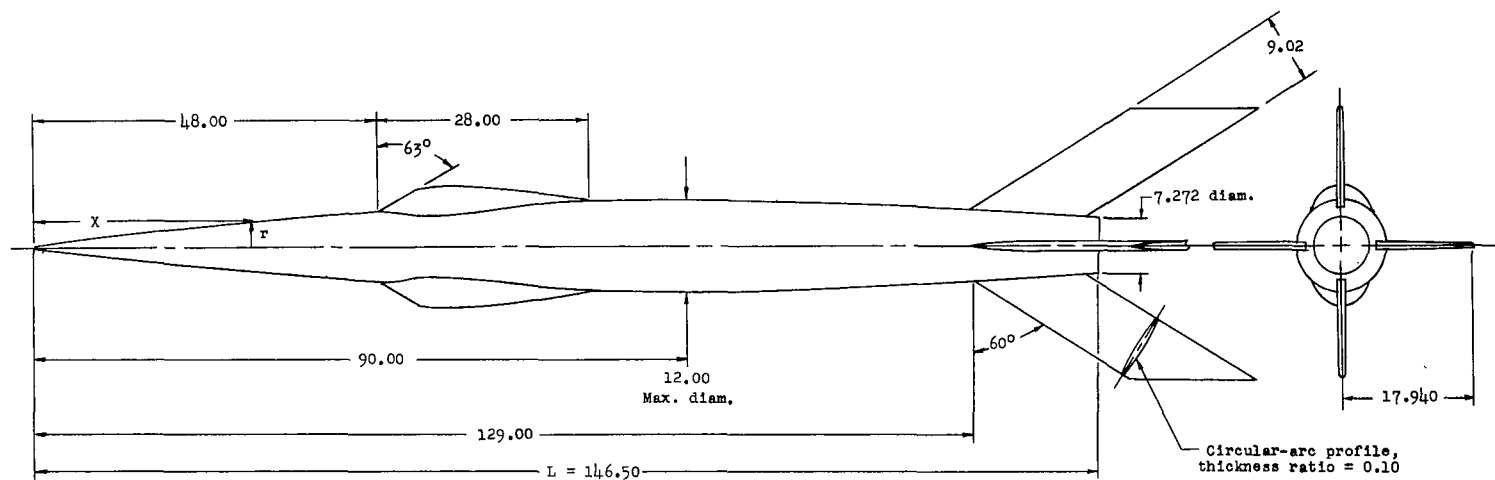
REFERENCES

1. Rumsey, Charles B., and Lee, Dorothy B.: Measurements of Aerodynamic Heat Transfer and Boundary-Layer Transition on a 10° Cone in Free Flight at Supersonic Mach Numbers up to 5.9. NACA RM L56B07, 1956.
2. Chauvin, Leo T., and Maloney, Joseph P.: Turbulent Convective Heat-Transfer Coefficients Measured From Flight Tests of Four Research Models (NACA RM-10) at Mach Numbers From 1.0 to 3.6. NACA RM L54L15, 1955.
3. Piland, Robert O., Collie, Katherine A., and Stoney, William E.: Turbulent and Laminar Heat-Transfer Measurements on a $1/6$ -Scale NACA RM-10 Missile in Free Flight to a Mach Number of 4.2 and to a Wall Temperature of 1400° R. NACA RM L56C05, 1956.
4. Maloney, Joseph P.: Drag and Heat Transfer on a Parabolic Body of Revolution (NACA RM-10) in Free Flight to Mach Number 2 With Both Constant and Varying Reynolds Number and Heating Effects on Turbulent Skin Friction. NACA RM L54D06, 1954.
5. Rumsey, Charles B.: Free-Flight Measurements of Aerodynamic Heat Transfer to Mach Number 3.9 and of Drag to Mach Number 6.9 of a Fin-Stabilized Cone-Cylinder Configuration. NACA RM L55G28a, 1955.
6. Rumsey, Charles B., and Lee, Dorothy B.: Measurements of Aerodynamic Heat Transfer and Boundary-Layer Transition on a 15° Cone in Free Flight at Supersonic Mach Numbers up to 5.2. NACA RM L56F26, 1956.
7. Bland, William M., Jr., and Collie, Katherine A.: Free-Flight Aerodynamic-Heating Data to Mach Number 10.4 for a Modified Von Kármán Nose Shape. NACA RM L56D25, 1956.
8. Dobbins, John P.: Development of Thermal Insulation for Jet Engine Exhaust Systems. Rep. No. NA-47-1122 (Contract NOa(s) 8474), North American Aviation Inc., Dec. 31, 1947.
9. Hoffman, Sherwood: Free-Flight Tests to Determine the Power-On and Power-Off Pressure Distribution and Drag of the NACA RM-10 Research Vehicle at Large Reynolds Numbers Between Mach Numbers 0.8 and 3.0. NACA RM L55H02, 1955.
10. Wallskog, Harvey A., and Hart, Roger G.: Investigation of the Drag of Blunt-Nosed Bodies of Revolution in Free Flight at Mach Numbers From 0.6 to 2.3. NACA RM L53D14a, 1953.

11. Robins, A. Warner: Force and Pressure Measurements on Several Canopy-Fuselage Configurations at Mach Numbers 1.41 and 2.01. NACA RM L55H23, 1955.
12. Van Driest, E. R.: The Turbulent Boundary Layer for Compressible Fluids on a Flat Plate With Heat Transfer. Rep. No. AL-997, North American Aviation, Inc., Jan. 27, 1950.
13. Rubesin, Morris W.: A Modified Reynolds Analogy for the Compressible Turbulent Boundary Layer on a Flat Plate. NACA TN 2917, 1953.
14. Hoffman Sherwood, and Robins, A. Warner: Drag of Canopies at Transonic and Supersonic Speeds. NACA RM L55L23, 1956.

TABLE I.- THICKNESS OF CANOPY SKIN
[Stations measured from canopy leading edge]

x/l	ϕ , deg	τ , in.
0.072	0	0.0310
.143	0	.0281
.143	9.9	.0300
.143	53.8	.0380
.214	0	.0281
.241	0	.0320
.241	34.3	.0319
.241	68.1	.0401
.429	0	.0341
.429	76.2	.0330
.643	0	.0360
.894	0	.0450

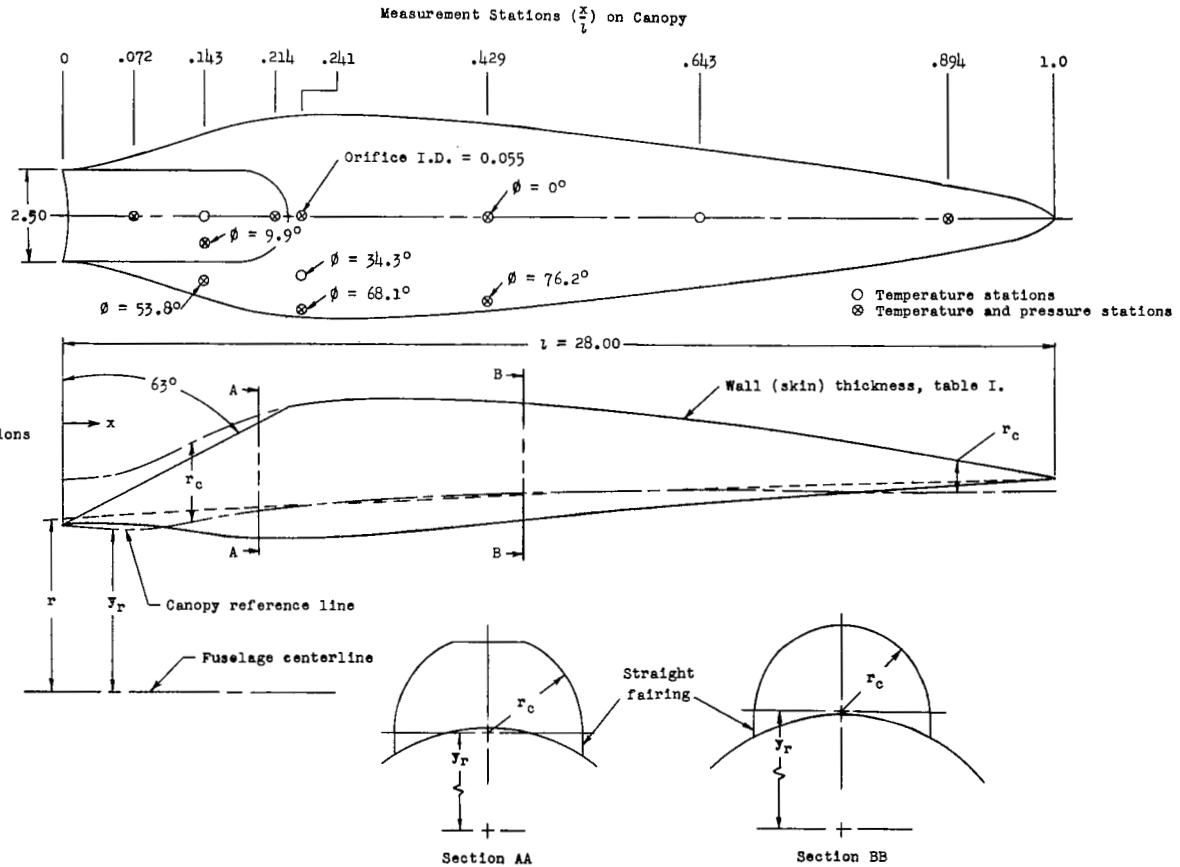
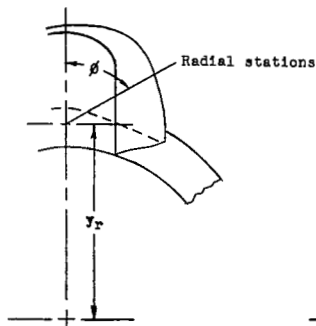


(a) General dimensions of model tested.

Figure 1.- Details and dimensions of model tested. All dimensions are in inches except where noted.

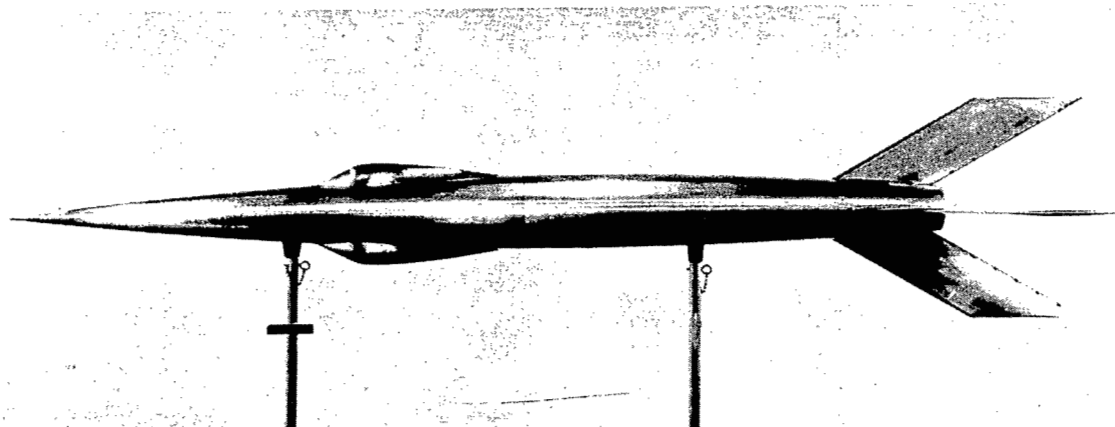
Contour Coordinate Table

x	r	r _c	y _r
0	4.69	1.25	4.50
1.0	4.76	1.39	4.44
2.0	4.82	1.65	4.40
3.0	4.87	1.95	4.49
4.0	4.93	2.25	4.67
5.0	4.99	2.51	4.85
6.0	5.04	2.70	4.99
7.0	5.09	2.78	5.09
8.0	5.14	2.79	5.17
9.0	5.19	2.76	5.24
10.0	5.24	2.70	5.30
12.0	5.33	2.55	5.39
14.0	5.42	2.35	5.46
16.0	5.50	2.12	5.50
18.0	5.57	1.87	5.53
20.0	5.64	1.63	5.52
22.0	5.70	1.39	5.50
24.0	5.76	1.09	5.47
26.0	5.81	.73	5.48
27.0	5.83	.53	5.50
28.0	5.86	.33	5.53



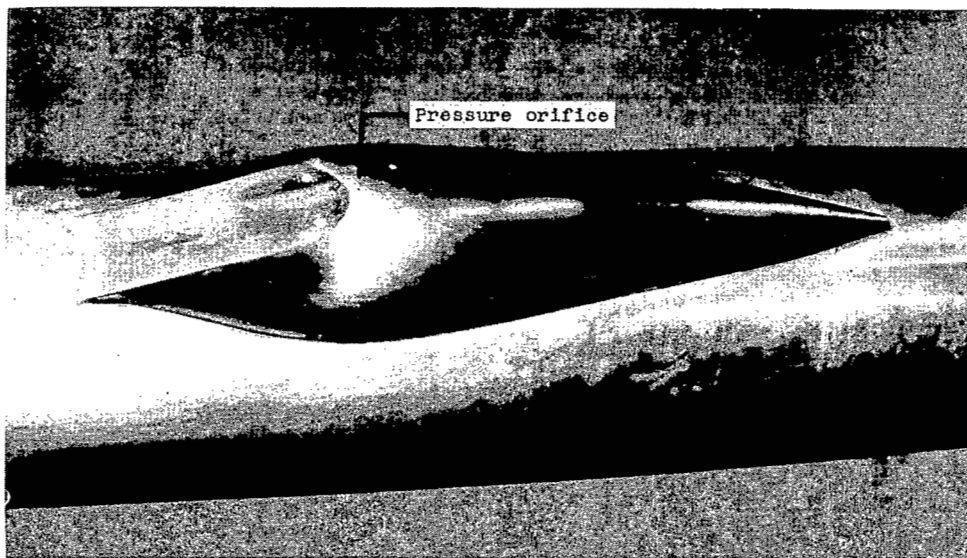
(b) Details of canopy.

Figure 1.- Concluded.



(a) Fuselage plus canopies.

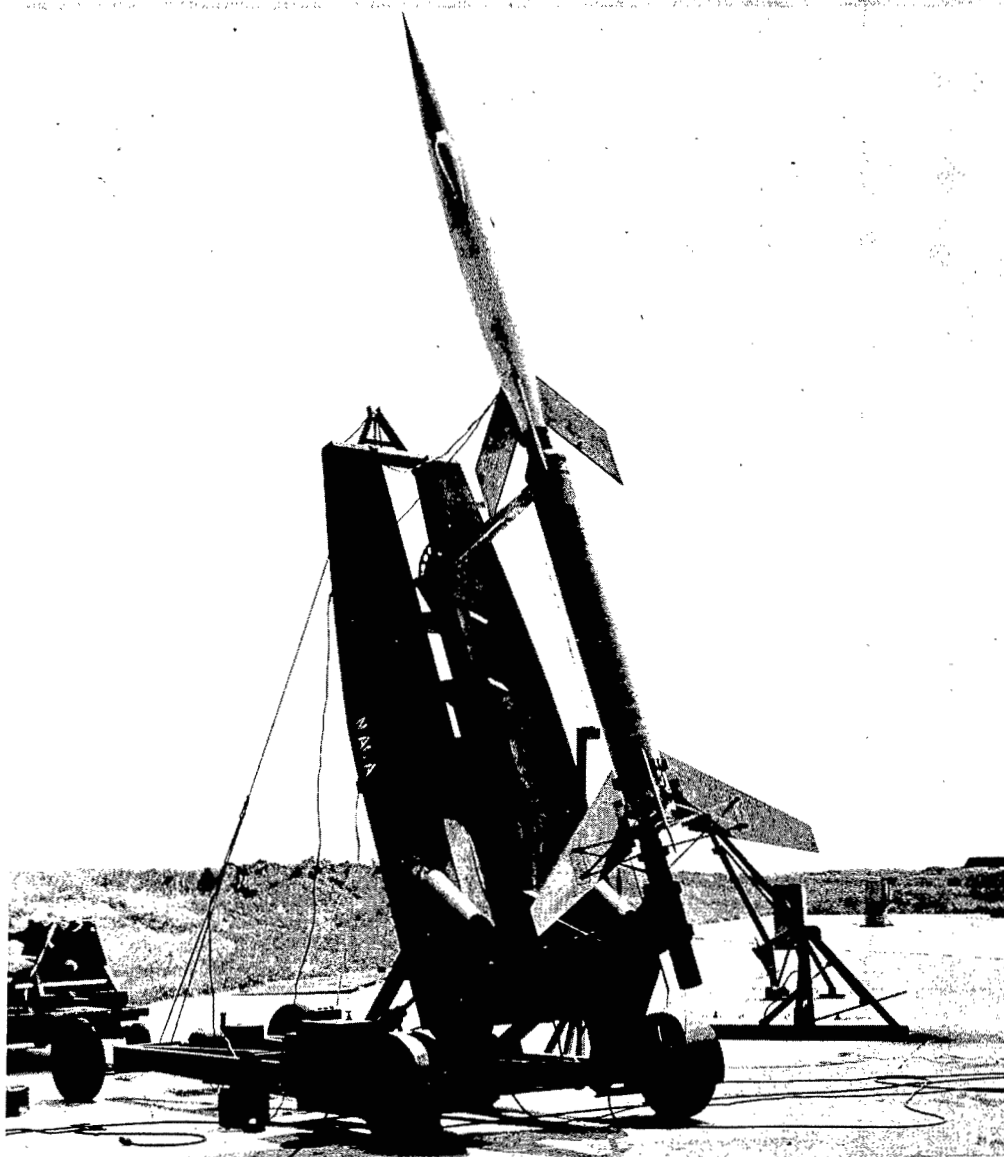
L-90363.1



(b) Closeup of canopy.

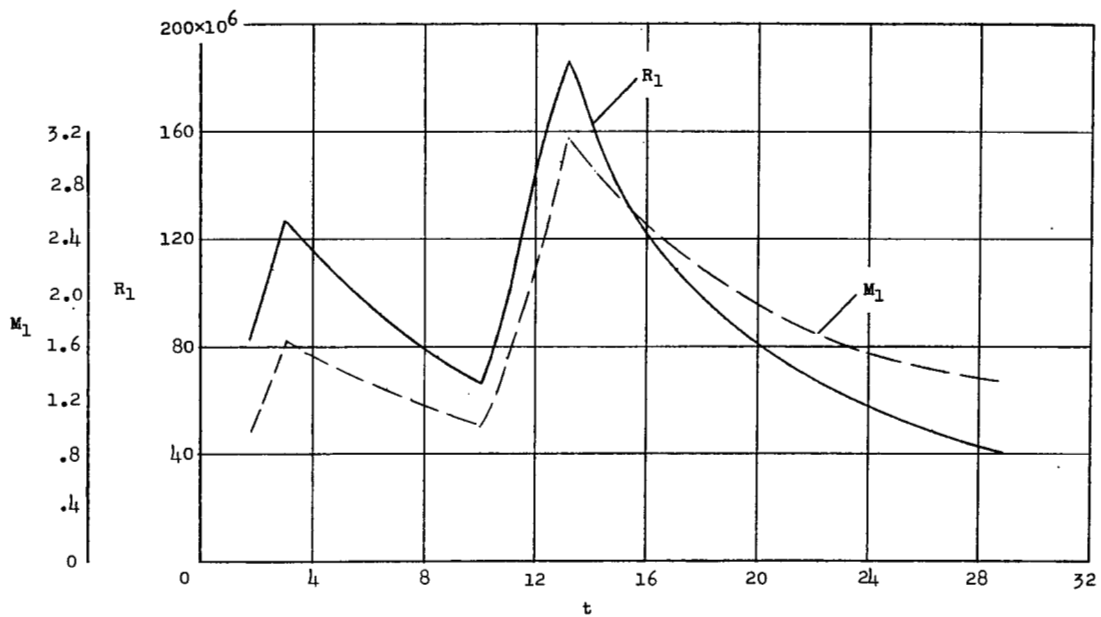
L-90362.1

Figure 2.- Photographs of model tested.

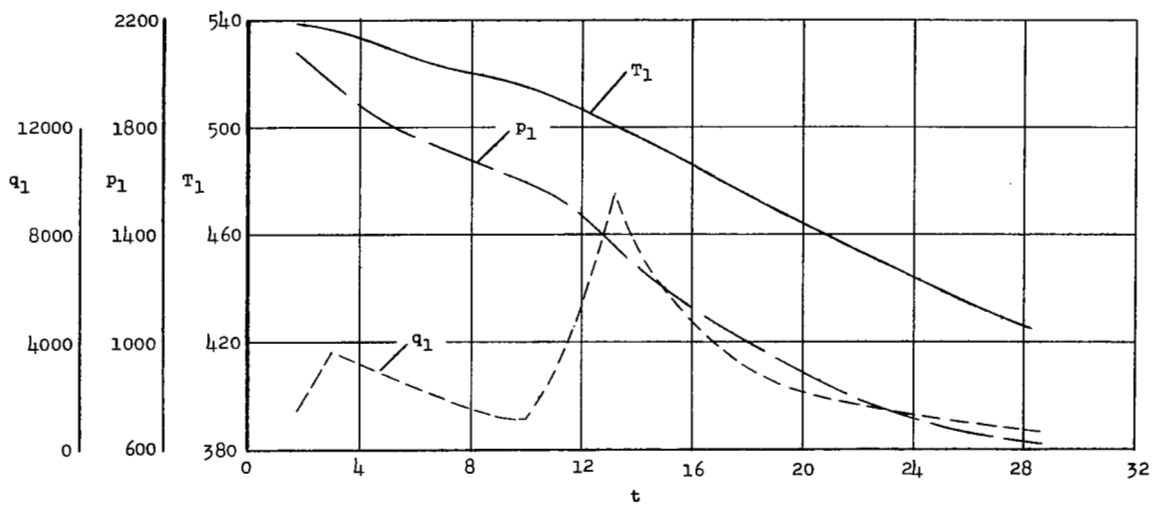


(c) Model and booster on launcher. L-90596

Figure 2.- Concluded.

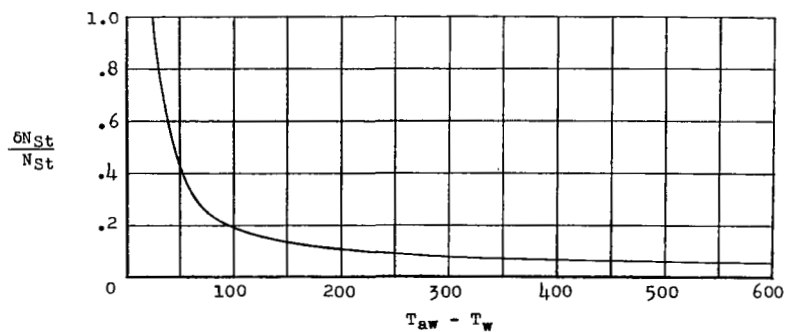


(a) Mach number and Reynolds number (based on fuselage length).

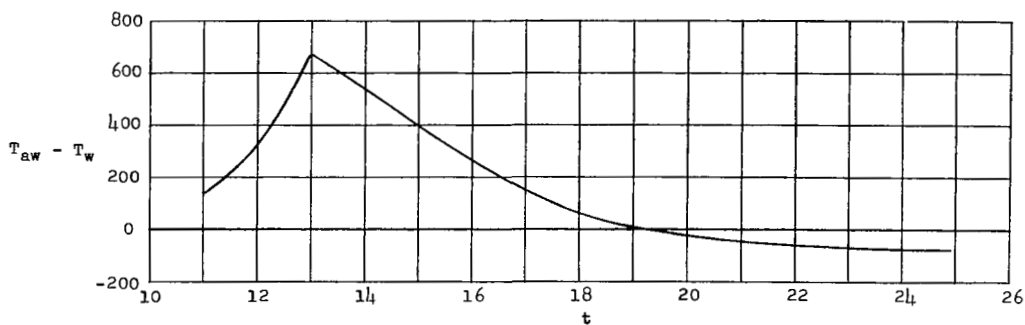


(b) Dynamic pressure, static pressure, and static temperature ($^{\circ}\text{R}$).

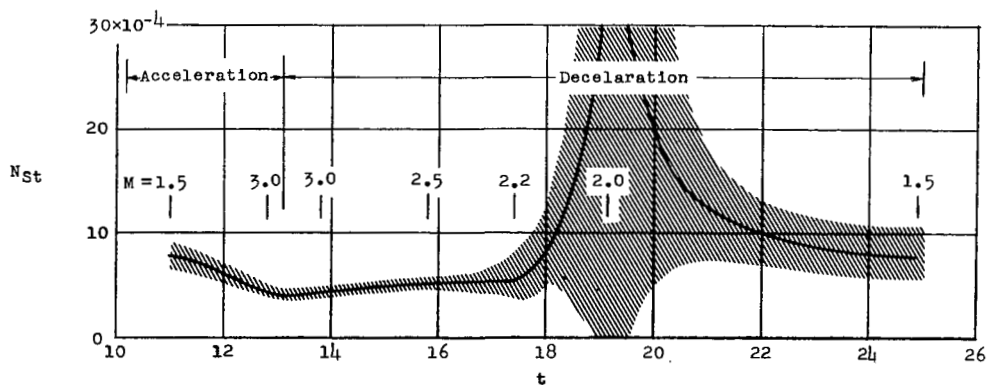
Figure 3.- Variations of free-stream conditions with time.



(a) Error in Stanton number as a function of heating potential.



(b) Heating potential at $x/l = 0.894$ and $\phi = 0^\circ$.



(c) Accuracy band and Stanton number at $x/l = 0.894$ and $\phi = 0^\circ$.

Figure 4.- Variation of probable error in Stanton number as a function of heating potential and an example of the accuracy obtained at a typical measuring station.

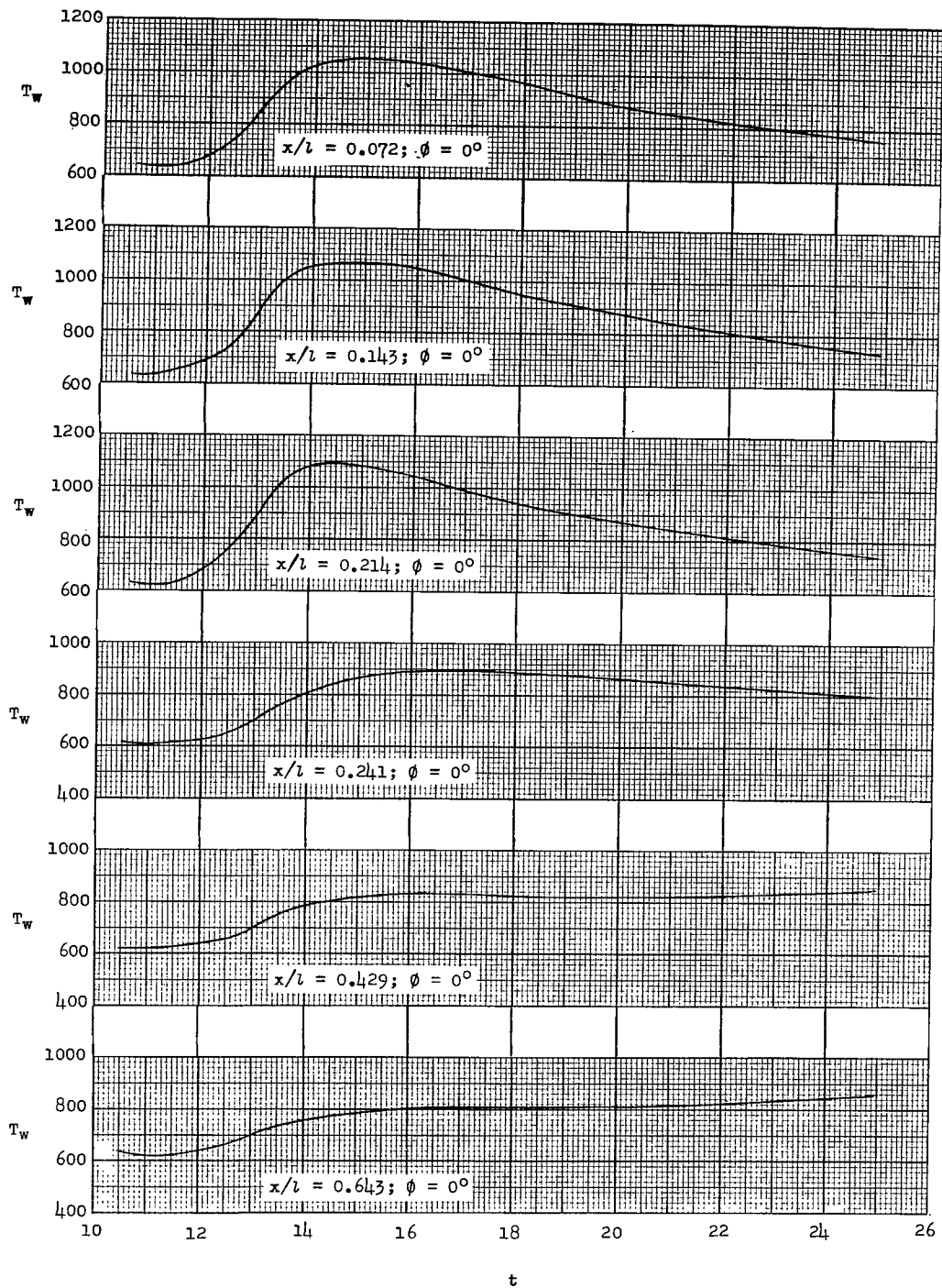


Figure 5.- Variations of wall temperature ($^{\circ}\text{R}$) with time at the canopy measuring stations.

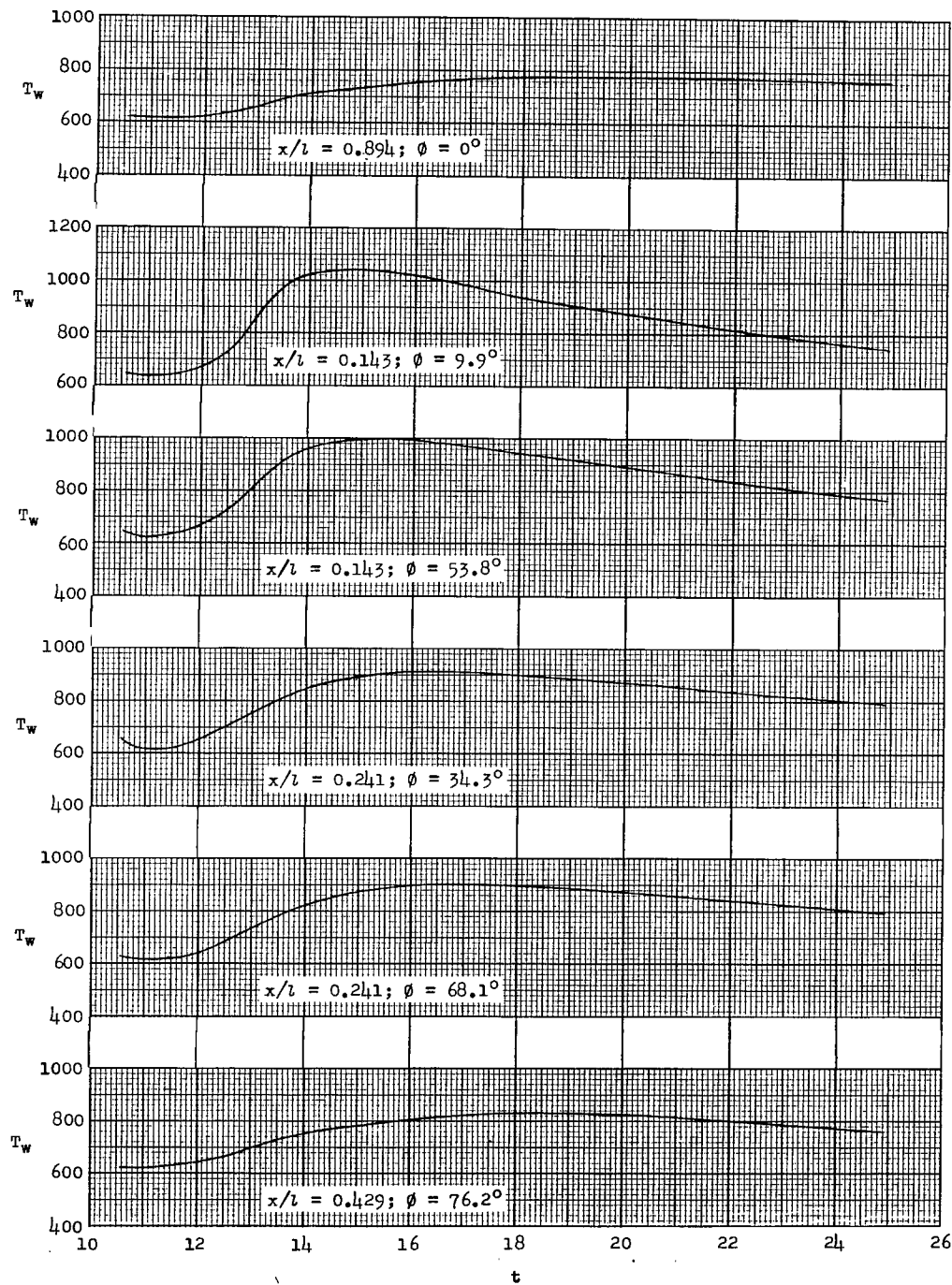
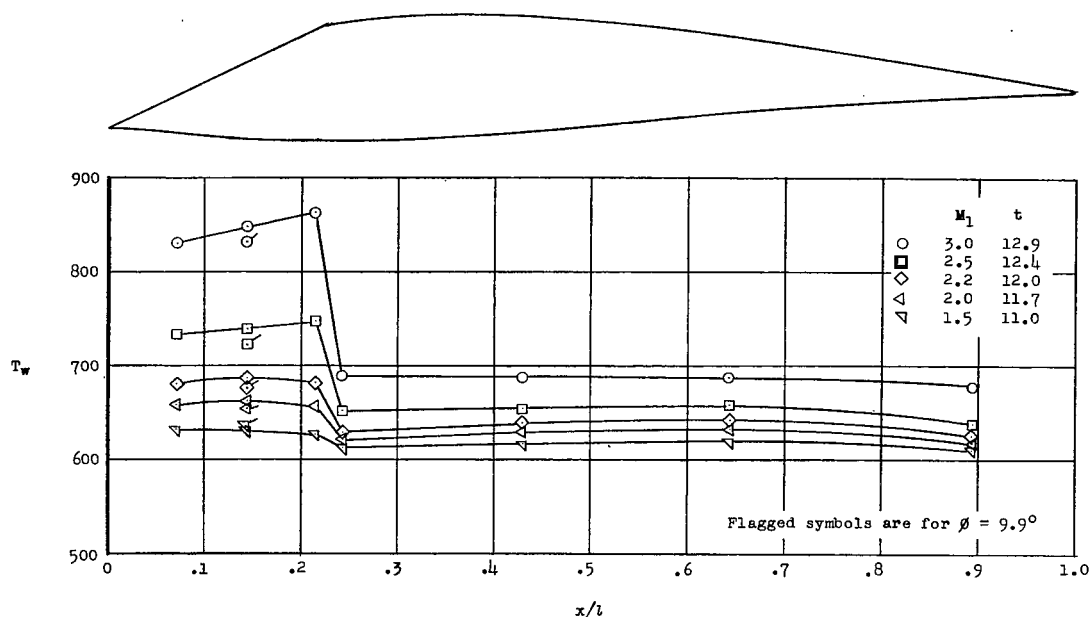
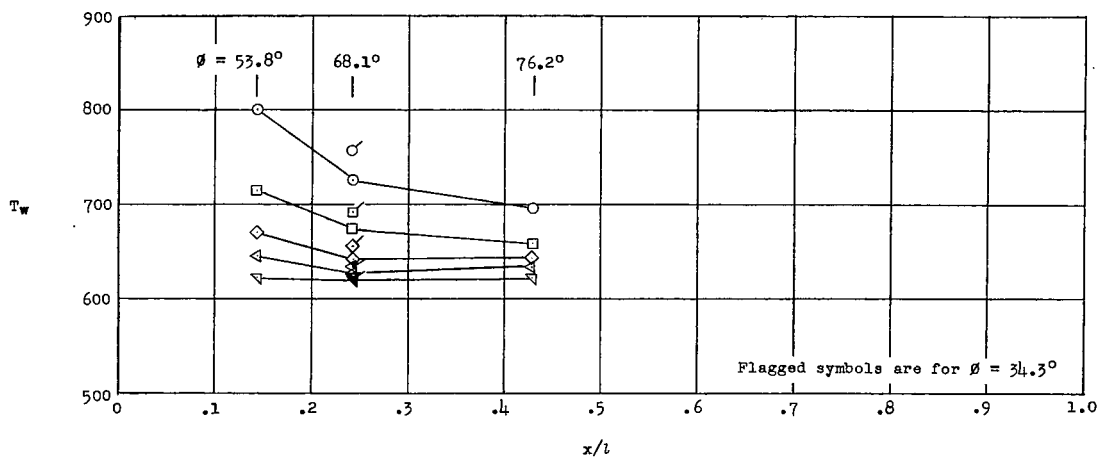


Figure 5.- Concluded.



(a) Wall temperature on top of canopy. $\phi = 0^\circ$ and 9.9° .



(b) Wall temperatures on side of canopy.

Figure 6.- Comparison of the distribution of wall temperature (°R) of the canopy at several Mach numbers during accelerated flight.

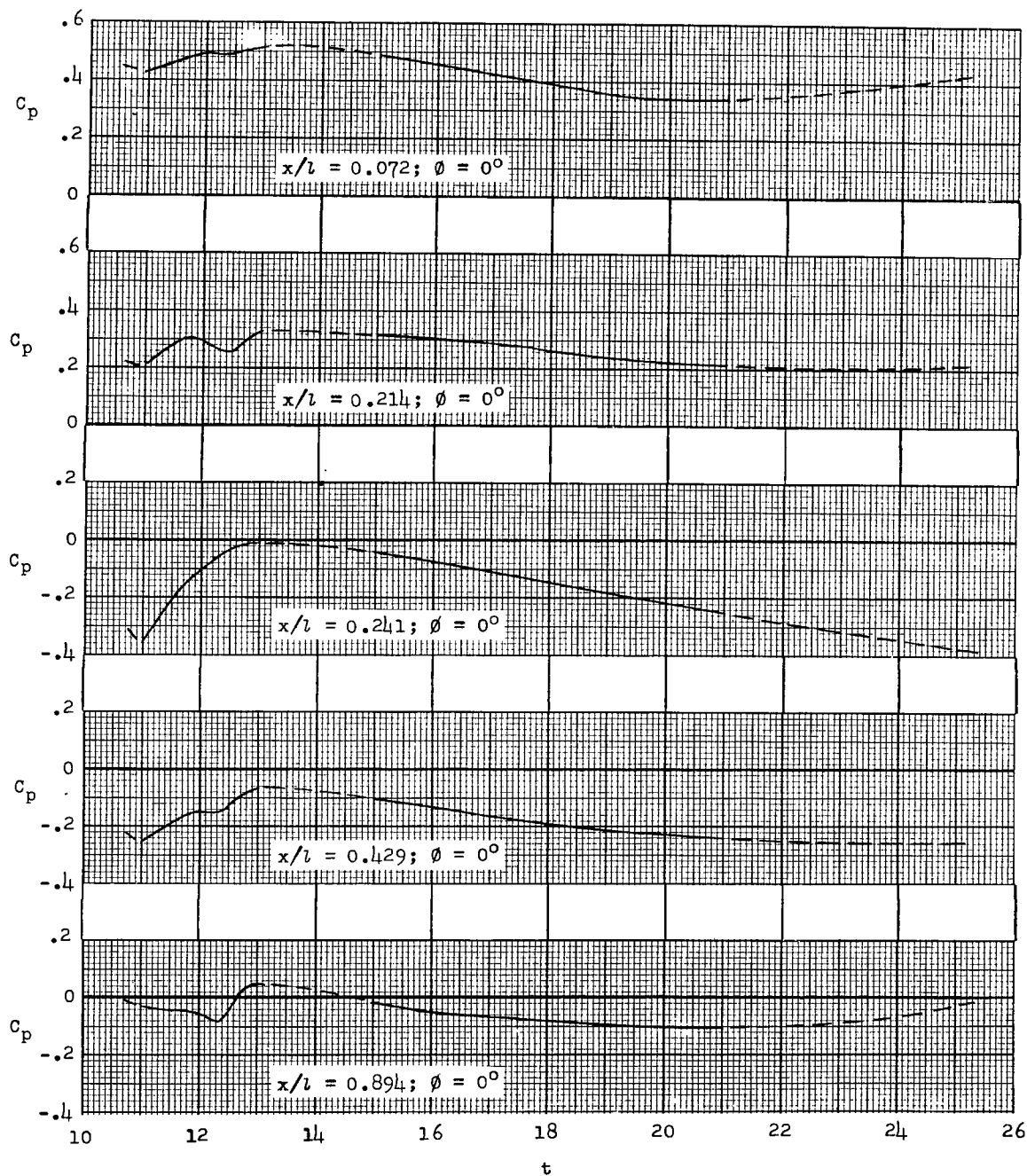


Figure 7.- Variations of pressure coefficients with time at the canopy measuring stations.

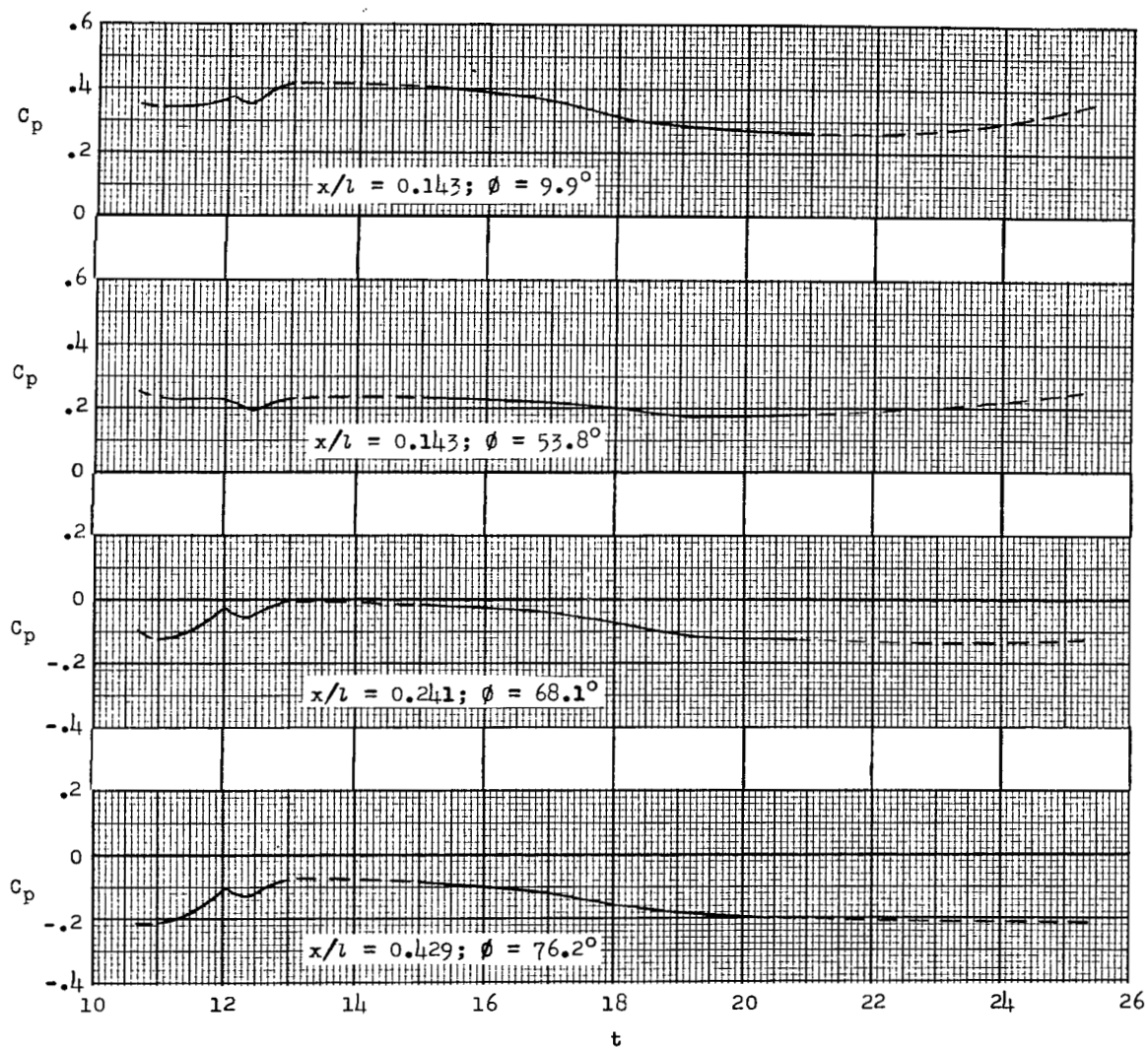
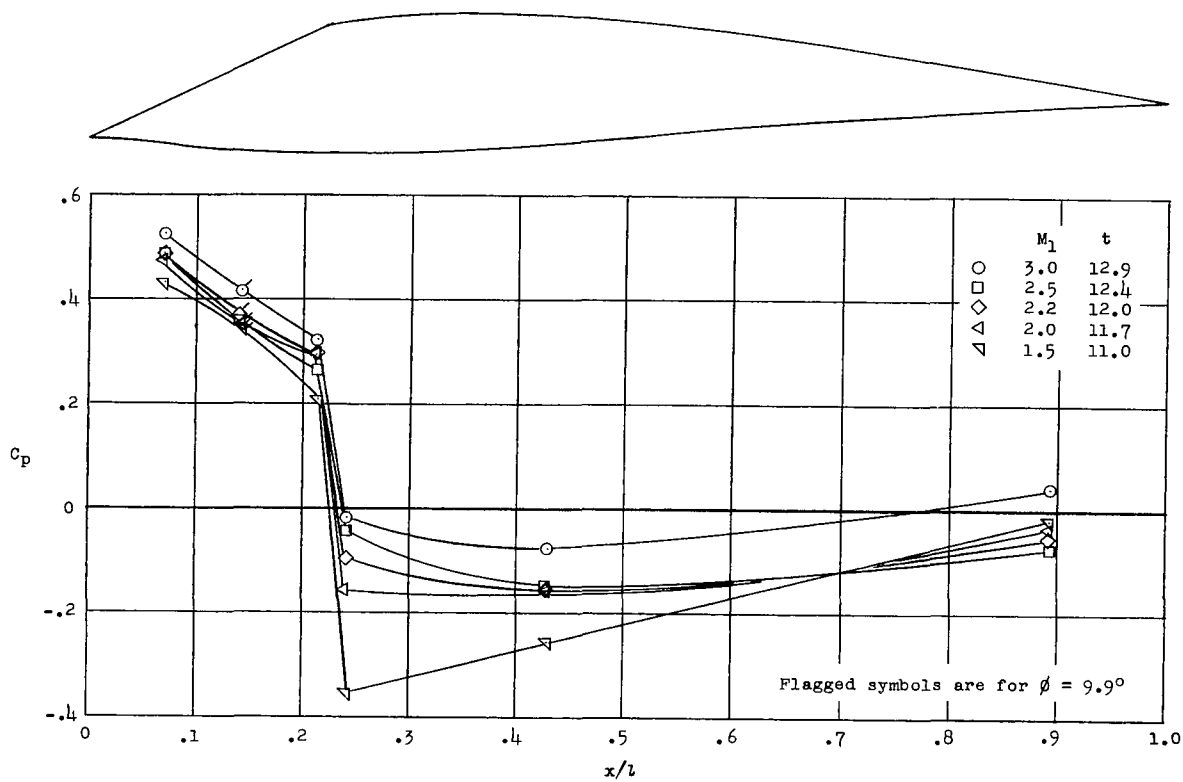
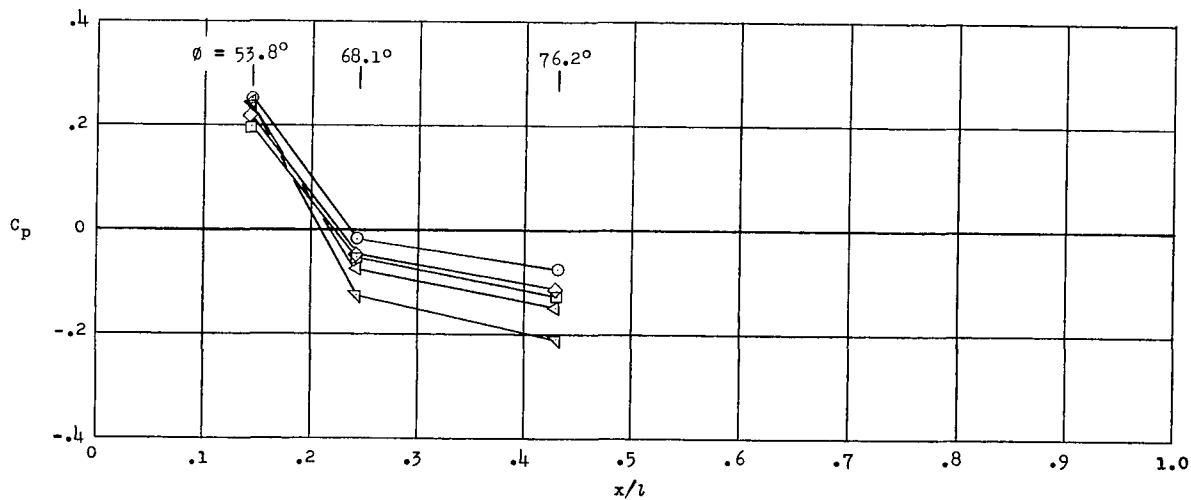


Figure 7.- Concluded.

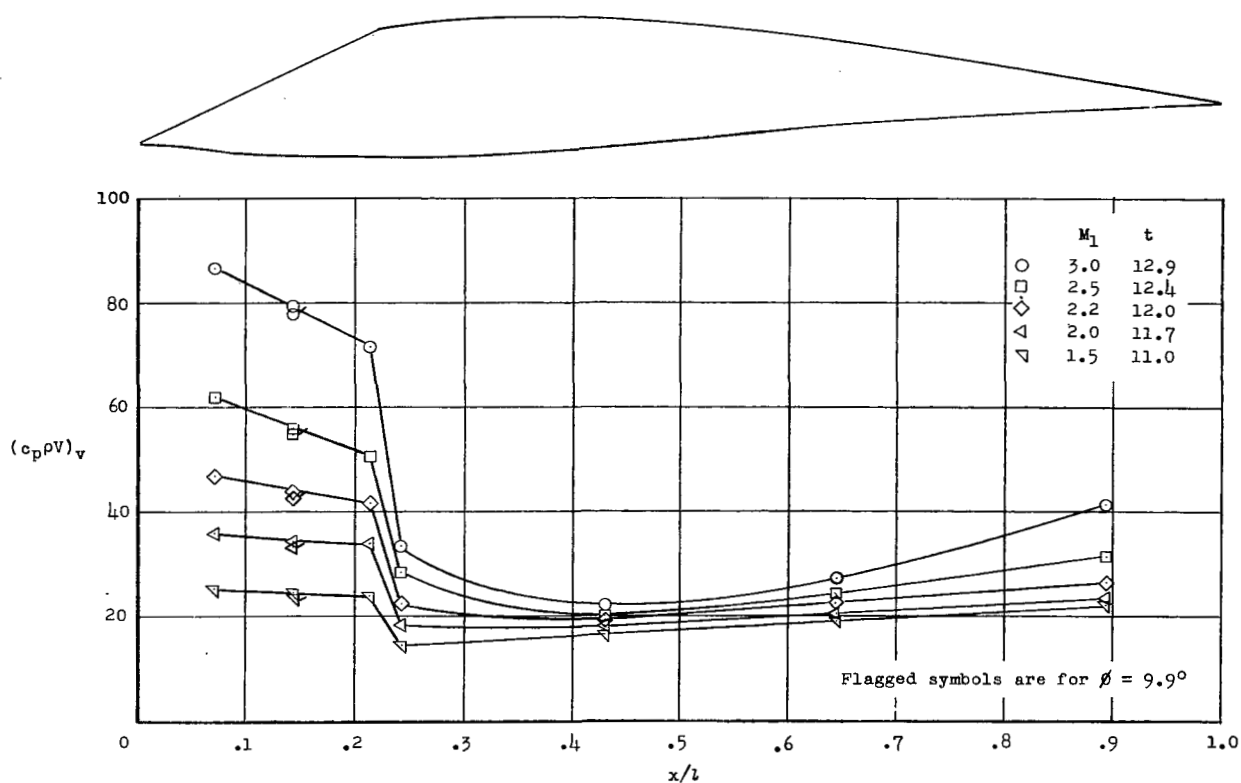
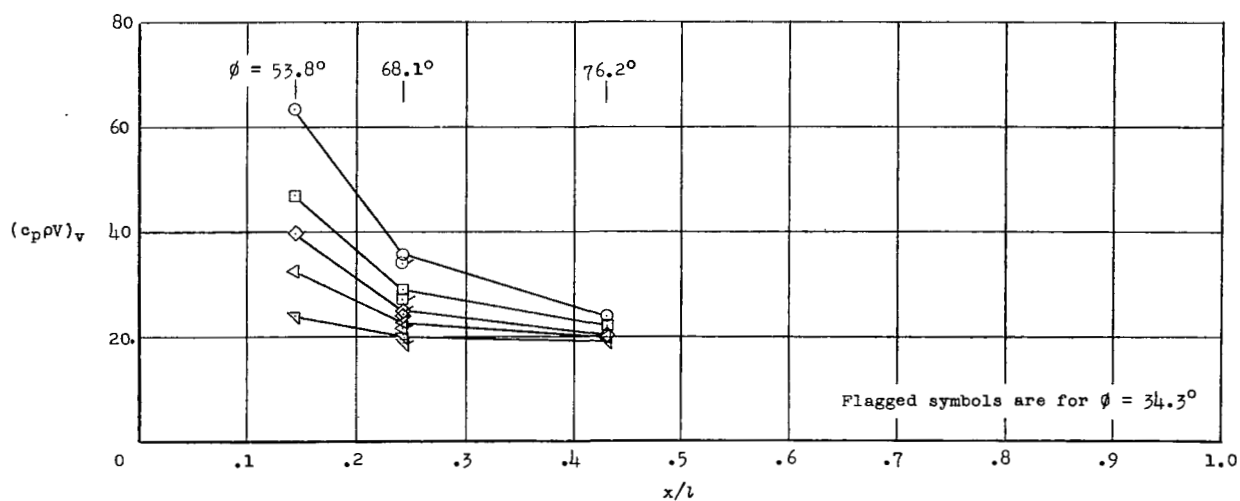


(a) Pressure coefficients on top of canopy. $\phi = 0^\circ$ and 9.9° .



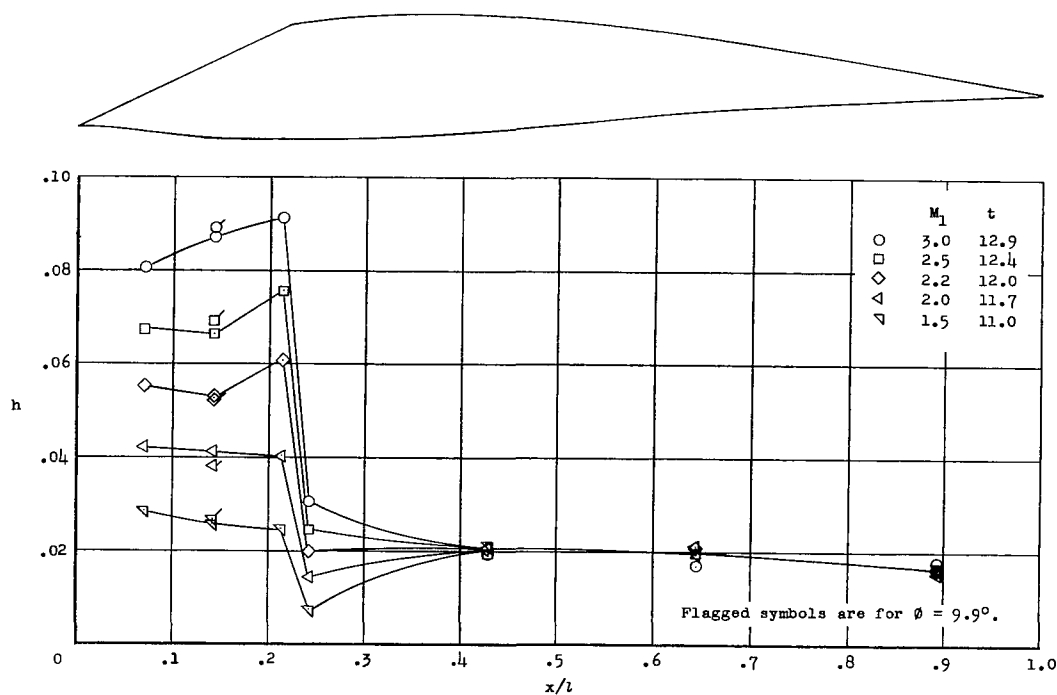
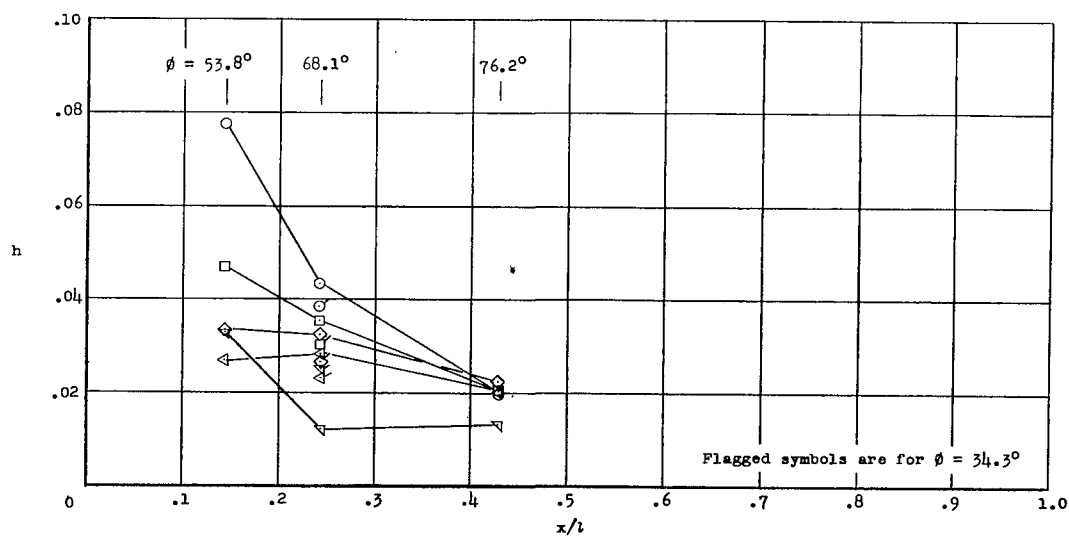
(b) Pressure coefficients on side of canopy.

Figure 8.- Comparison of the distribution of pressure coefficient of the canopy at several Mach numbers during accelerated flight.

(a) Top of canopy. $\phi = 0^\circ$ and 9.9° .

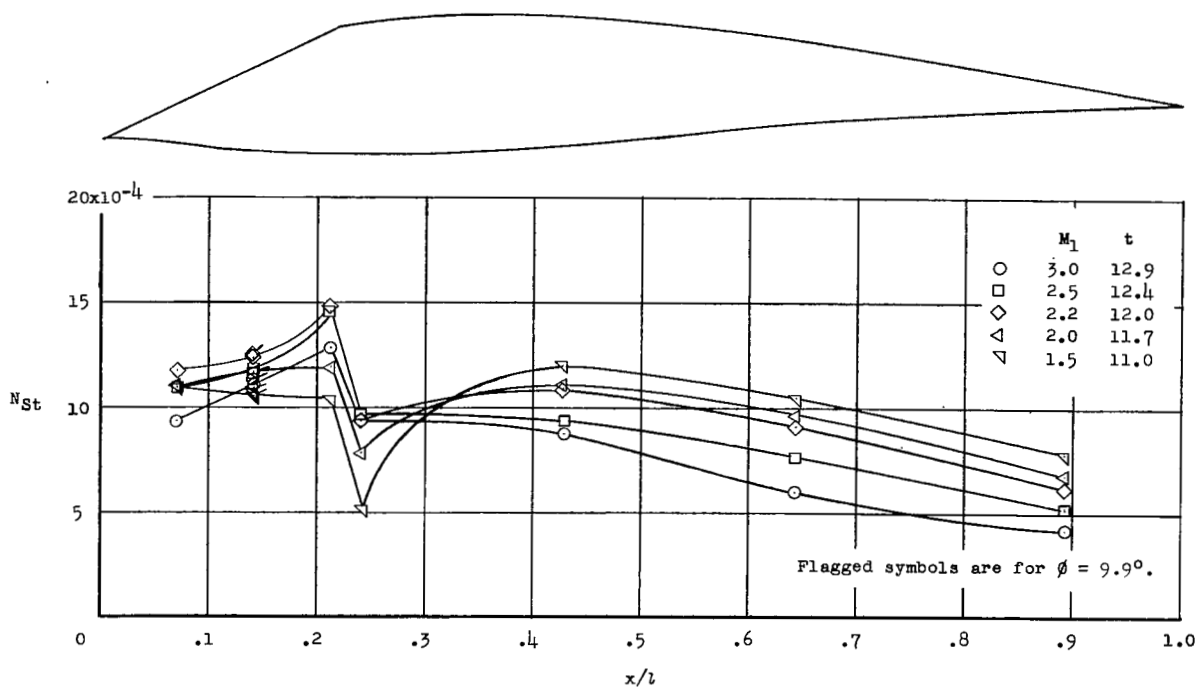
(b) Side of canopy.

Figure 9.- Comparison of the distribution of $(c_p \rho V)_v$ of the canopy at several Mach numbers during accelerated flight.

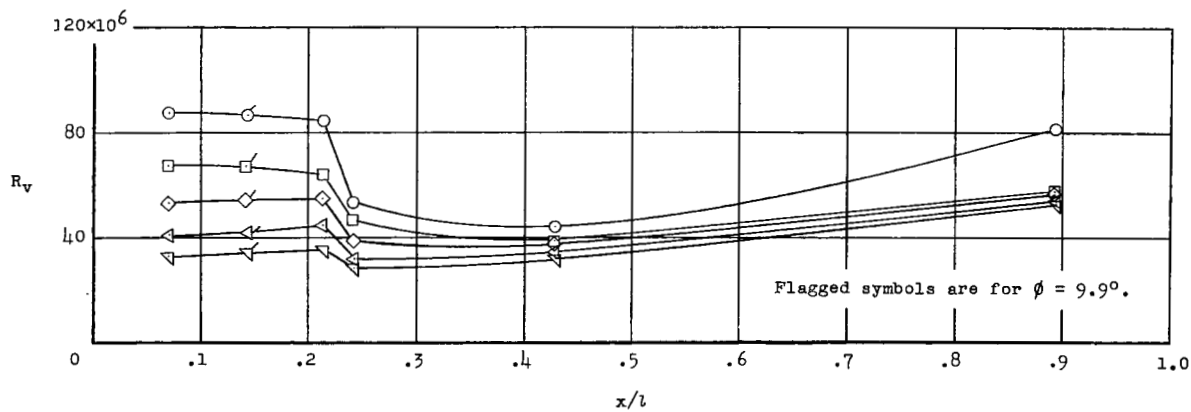
(a) Top of canopy. $\phi = 0^\circ$ and 9.9° .

(b) Side of canopy.

Figure 10.- Comparison of the distribution of heat-transfer coefficient for the canopy at several Mach numbers during accelerated flight.

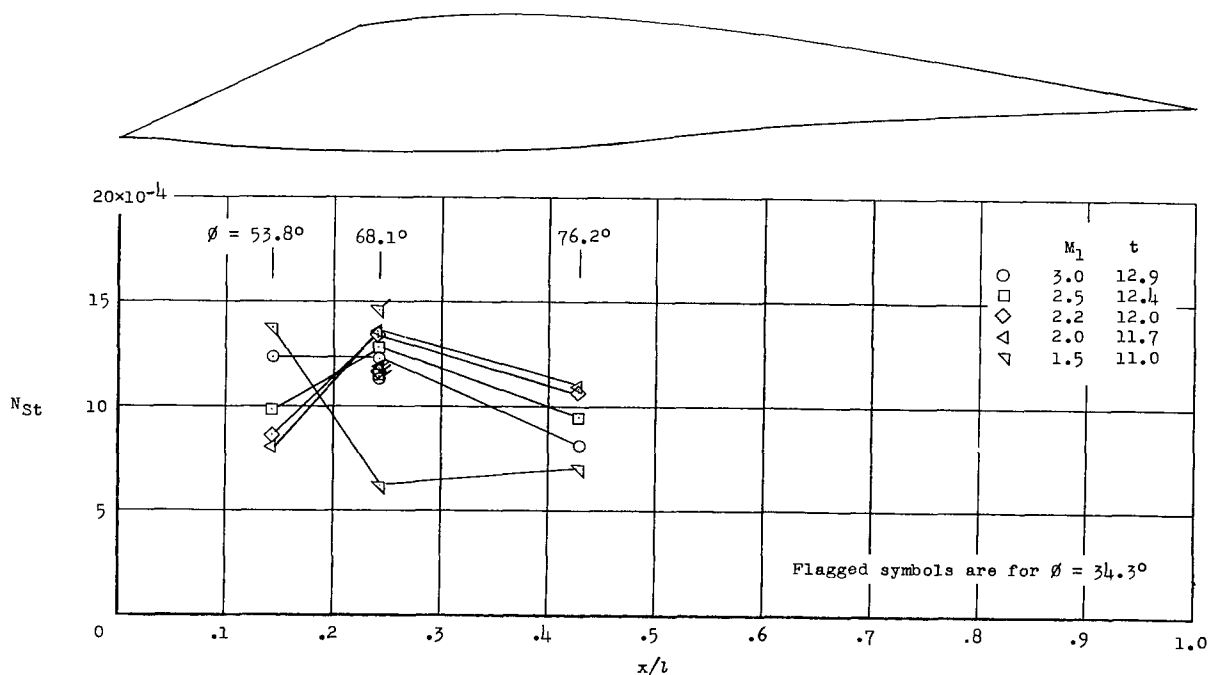


(a) Stanton number.

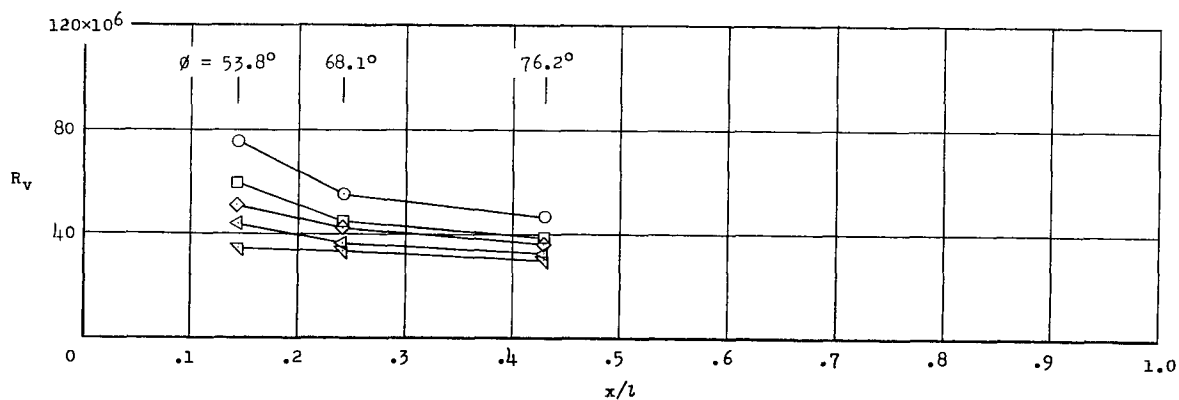


(b) Local Reynolds number.

Figure 11.- Comparisons of the distributions of Stanton number and Reynolds number on the top of the canopy at $\phi = 0^\circ$ and 9.9° for several Mach numbers during accelerated flight.



(a) Stanton number.



(b) Local Reynolds number.

Figure 12.- Comparisons of the distributions of Stanton number and Reynolds number on the side of the canopy for several Mach numbers during accelerated flight.

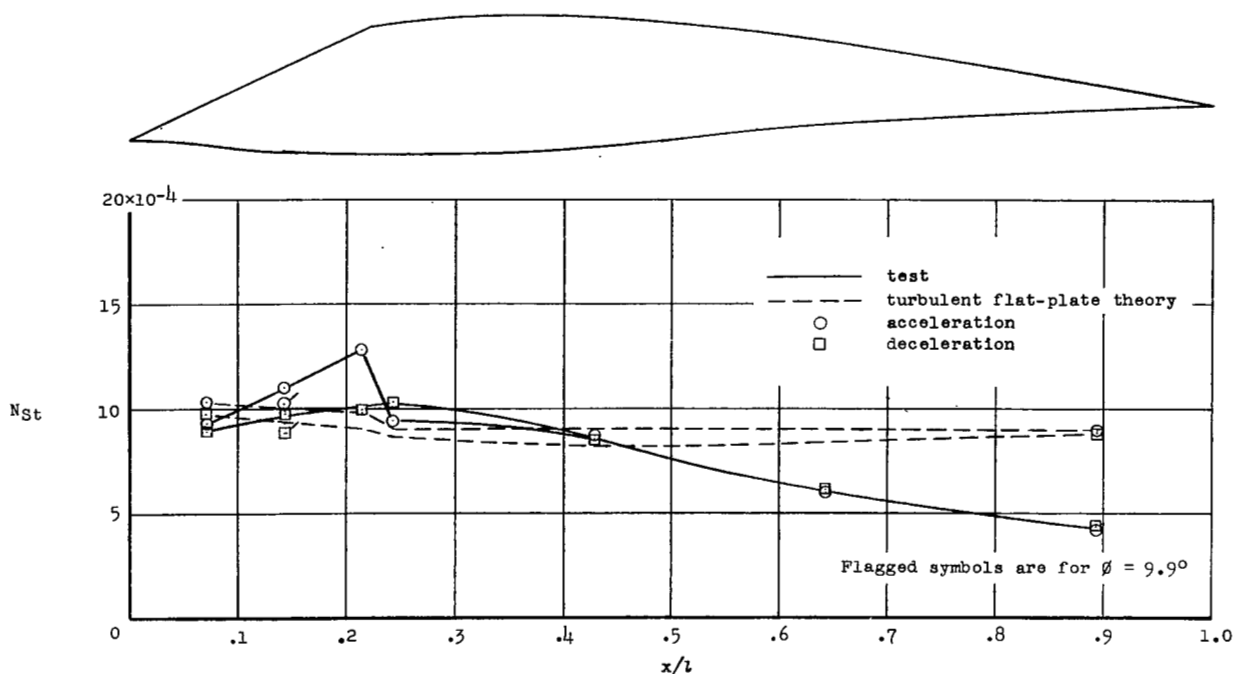
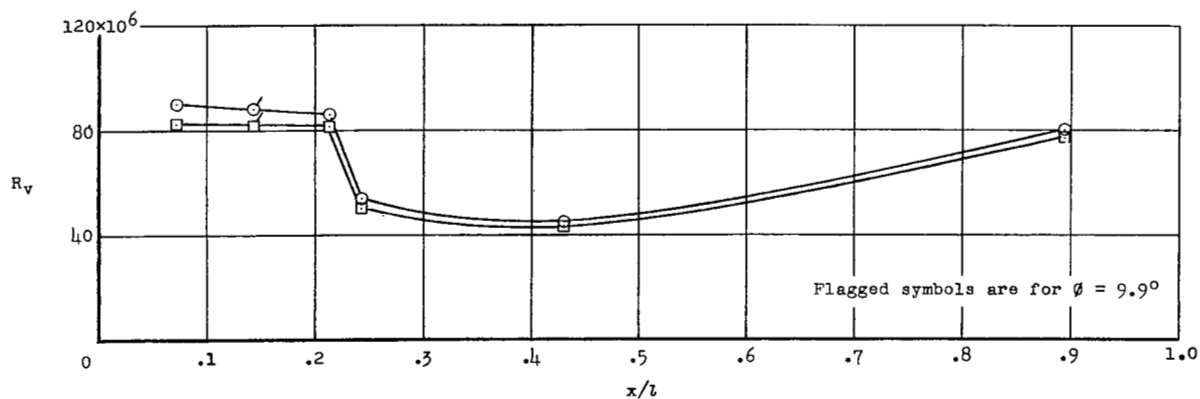
(a) Stanton number at $M_1 = 3.0$.(b) Local Reynolds number at $M_1 = 3.0$.

Figure 13.- Comparisons of the Stanton numbers as obtained from the test and turbulent flat-plate theory, and Reynolds number on the top of the canopy ($\phi = 0^\circ$ and 9.9°) for several Mach numbers during accelerated and decelerated flight.

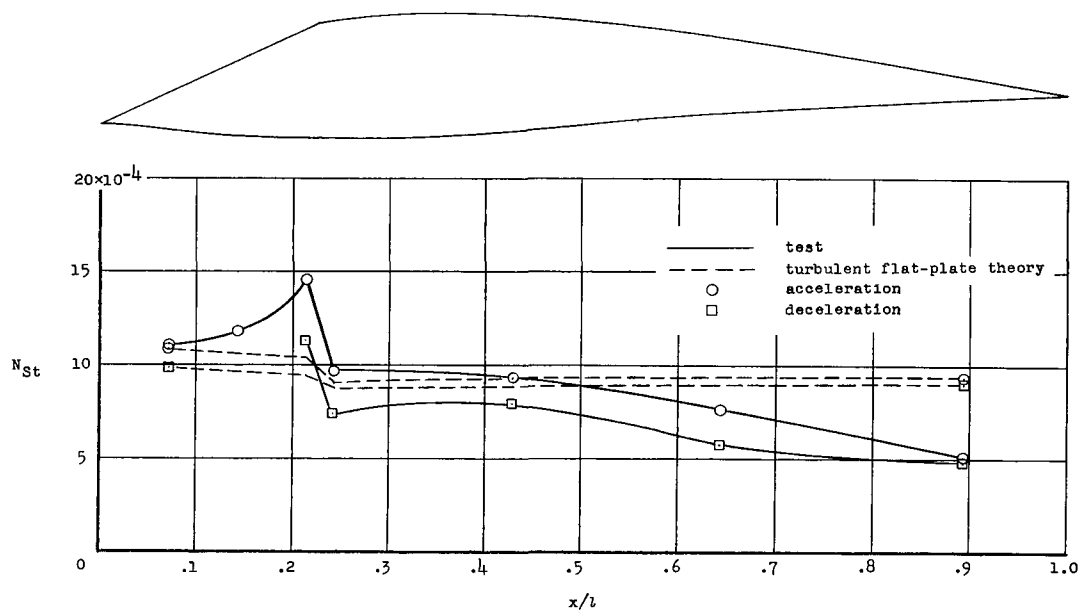
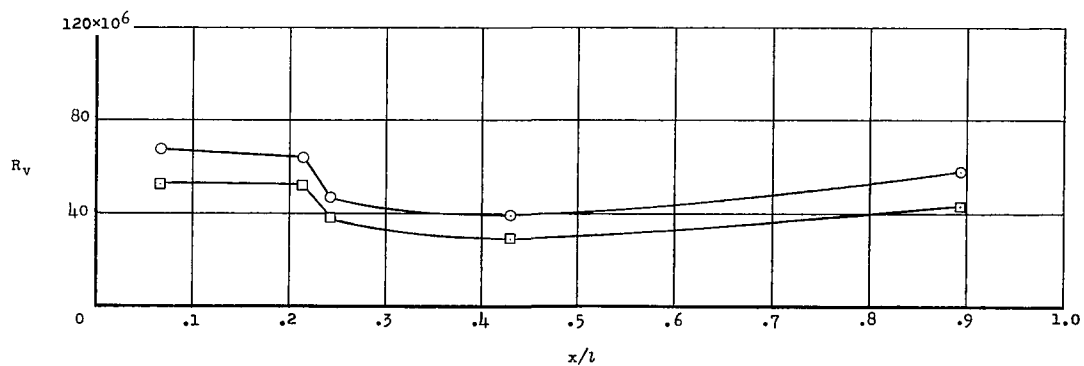
(c) Stanton number at $M_1 = 2.5$.(d) Local Reynolds number at $M_1 = 2.5$.

Figure 13.- Continued.

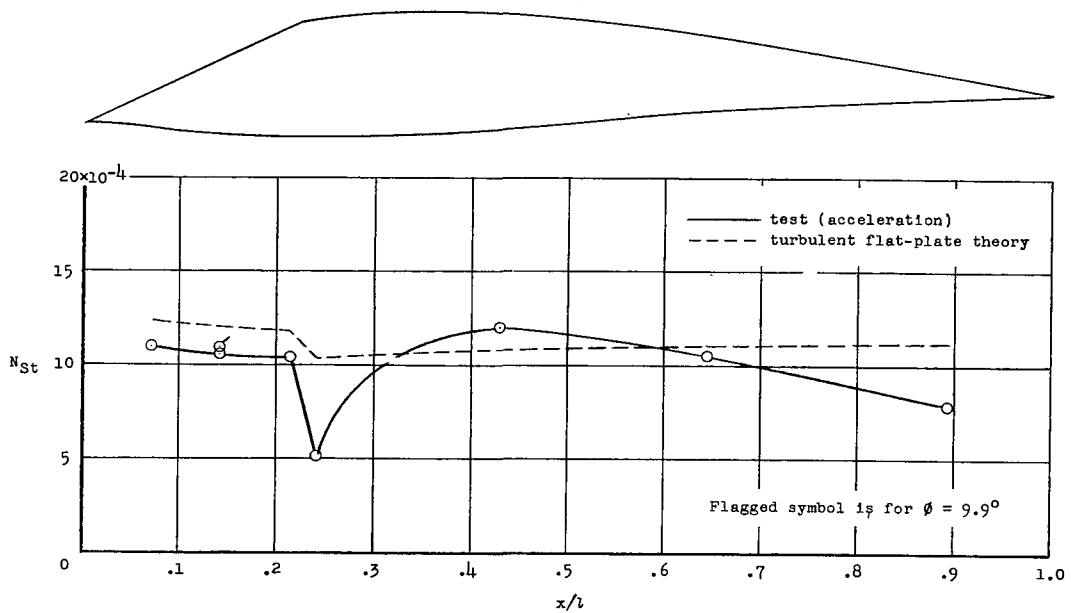
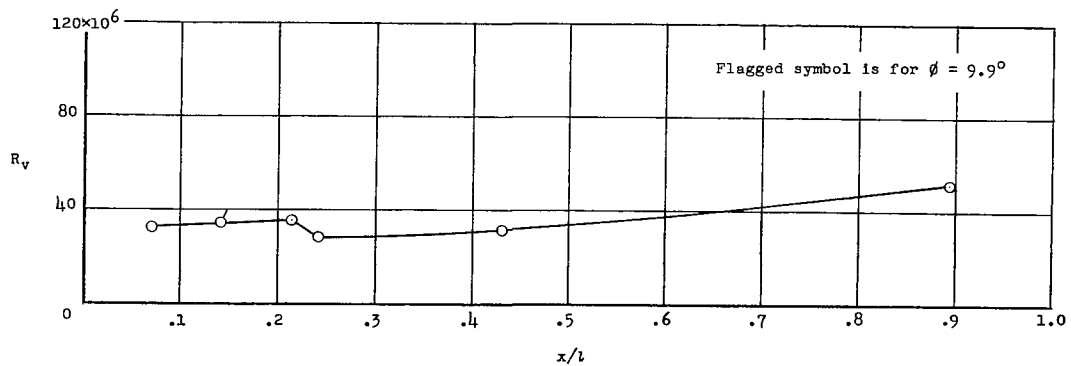
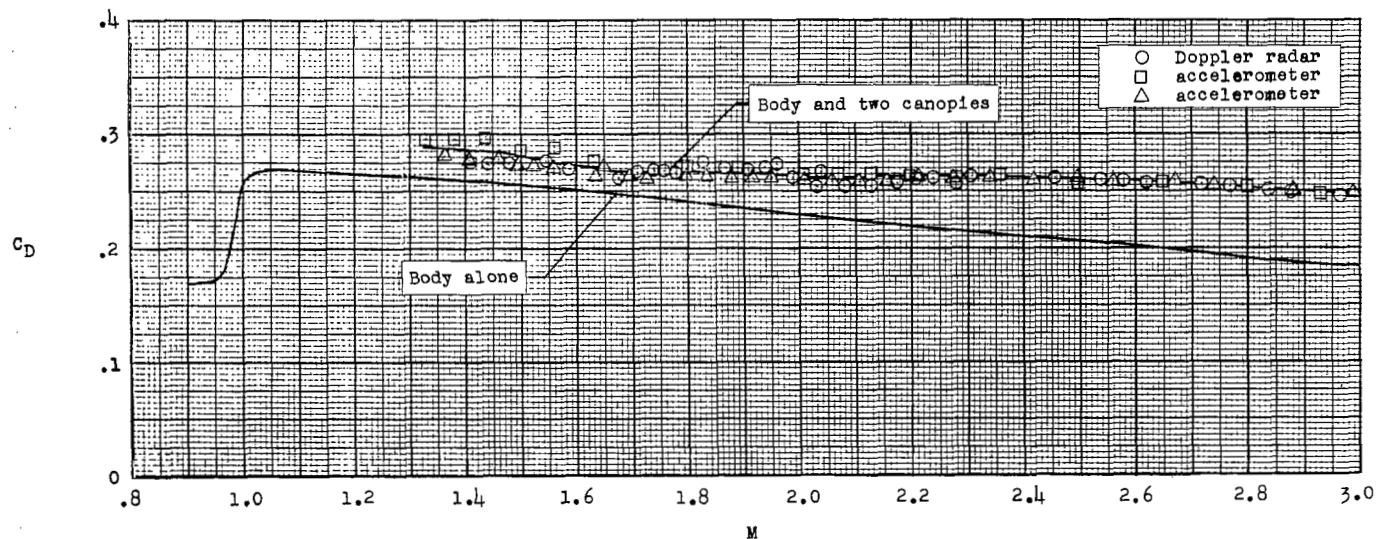
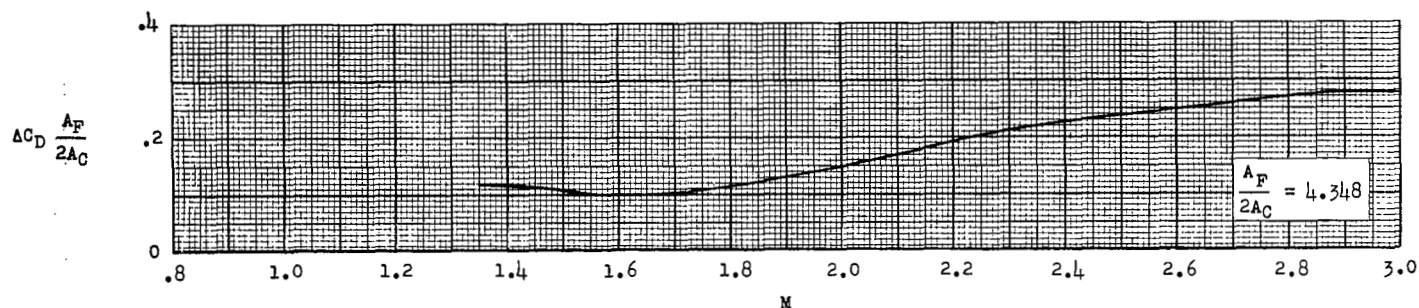
(e) Stanton number at $M_1 = 1.5$.(f) Local Reynolds number at $M_1 = 1.5$.

Figure 13.- Concluded.



(a) Total drag coefficient.



(b) Canopy plus interference drag coefficient.

Figure 14.- Variations of total drag coefficient and canopy plus interference drag coefficient with Mach number.

NASA Technical Library



3 1176 01437 2388

CONFIDENTIAL